Electromagnetic interactions of cosmic-ray muons at large zenith angles at sea level

1971 J. Phys. A: Gen. Phys. 4 649

(http://iopscience.iop.org/0022-3689/4/5/007)

J. Phys. A: Gen. Phys., 1971, Vol. 4. Printed in Great Britain

Electromagnetic interactions of cosmic-ray muons at large zenith angles at sea level

F. ASHTON and R. B. COATS
Department of Physics, University of Durham, England
MS. received 18*th March* 1971

Abstract. The electromagnetic interactions of cosmic-ray muons incident at sea level in the zenith angle range 50–90° have been studied. The measurements cover energy transfers from 3 to 240 GeV produced by muons in the energy range 34 to 520 GeV. No significant divergence from accepted theory has been found.

1. Introduction

Although there have been many studies of the cosmic-ray beam in the vertical direction at sea level comparatively few measurements have been made at large zenith angles. The pioneer experiment of Jakeman (1956) established the existence of a nearly horizontal flux of muons at sea level, and subsequently the momentum spectrum of muons at large zenith angles was measured by Allen and Apostolakis (1961), Ashton and Wolfendale (1963) and Ashton *et al.* (1966). The present experiment was undertaken to study the interaction characteristics of high energy particles at zenith angles greater than 50° at sea level, preliminary results having already been reported (Ashton and Coats 1965, Ashton *et al.* 1968).

2. Experimental arrangement

The experimental arrangement used is shown in figure 1. F1 and F2 are iron

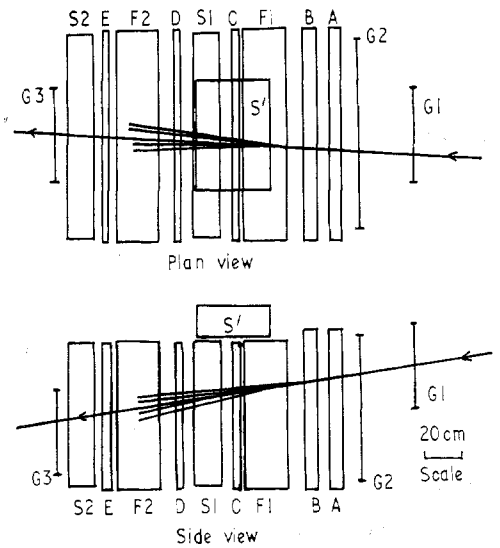

Figure 1. Scale diagram of the apparatus. G: geiger counters; A, B, C, D, E: flash tubes; S1, S2, S′: scintillation counters; F1, F2: iron. G1 and G3 are only used to calibrate the scintillation counters in terms of their response to the passage of single relativistic muons.

targets, each of thickness 25 cm (13·7 radiation lengths) and S1, S2 are liquid scintillation counters each of area 1·24 m^2 of the type described by Ashton *et al.* (1965). Events were selected in which a high energy muon traversed geiger counter tray G2 and underwent a large energy transfer (producing a high energy knock-on electron, bremsstrahlung photon, positron–electron pair, or a nuclear interaction) in F1 or F2, the resulting electron–photon shower being detected by S1 or S2. Bursts of more than n equivalent particles (1 equivalent particle is defined as the average pulse height produced by relativistic muons traversing either scintillator at normal incidence relative to its largest area) traversing S1 or S2 were detected independently by the selection system G2, S1 ($> n$), $\bar{S}'$ and G2 . S2($> n$) . $\bar{S}'$. The anticoincidence scintillator S′ is necessary to cut down the large background of extensive air showers that would otherwise trigger the apparatus. The neon flash tube trays A, B, C, D, E clearly indicate genuine burst events and without this facility the present experiment would not have been possible. For each burst event the zenith angle of the incident

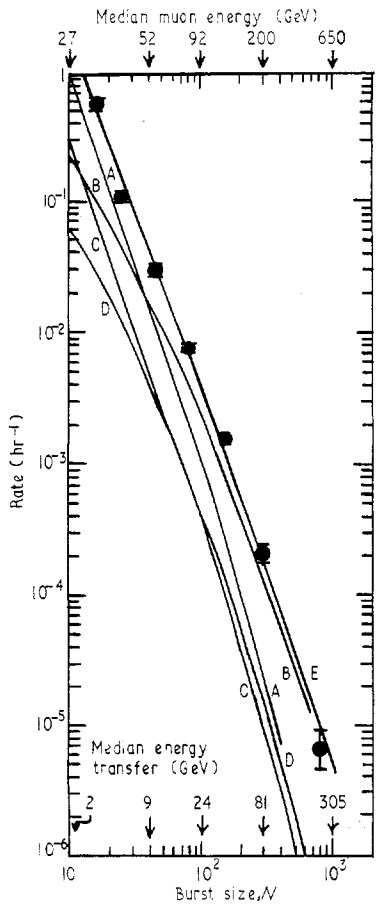

Figure 2. The measured differential burst spectrum in S1 and comparison with expectation. Zenith angle range of incident muons 50–90 °. A, μ–e collisions; B, bremsstrahlung; C, e^+e^- pairs; D, nuclear interactions; E, total.

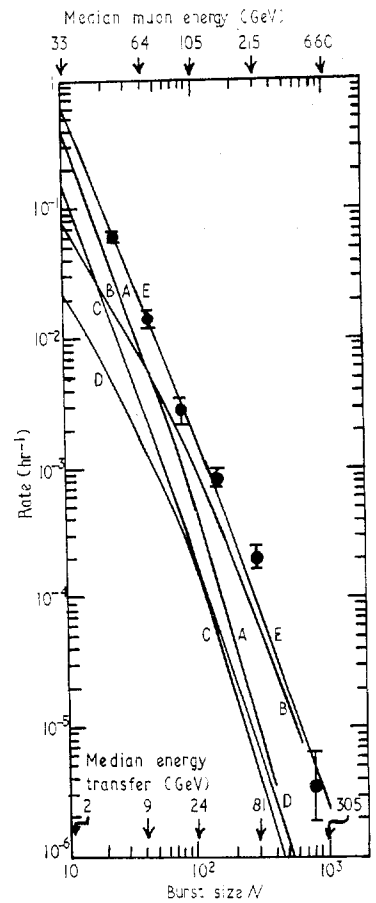

Figure 3. The measured differential burst spectrum in S2 and comparison with expectation. Zenith angle range of incident muons 63–90 °. A–E as for figure 2.

muon, the spatial position of the axis of the burst traversing C, D or E flash tube layers, and the voltage pulse height recorded by the scintillation counters were measured. This pulse height, which is a measure of the total track length of ionizing particles in the scintillator, is then converted to the relevant number of equivalent particles. The equivalent particle calibration is done using the selection system G1.G2. G3, $\bar{S}'$.

The apparatus has been operated for a period of 1931 h selecting bursts produced in F1, and for 1442 h selecting bursts produced in F2. The measured differential burst spectra recorded by S1 and S2 for all accepted zenith angles are

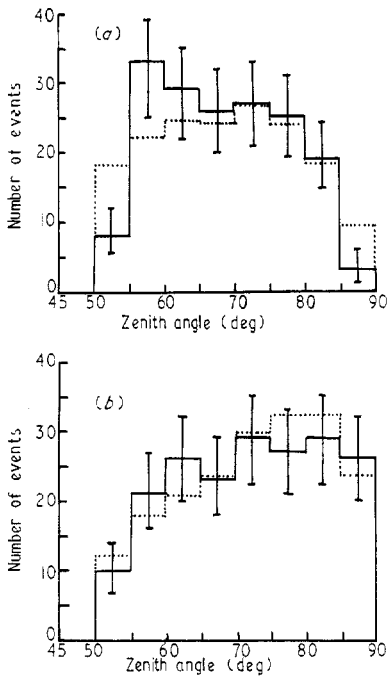

Figure 4. Angular distribution of bursts of size (*a*) 10–20 and (*b*) 100–200 equivalent particles measured in S1. The statistical accuracy of the number of events in each cell is represented by the error flag. The broken line is the predicted distribution.

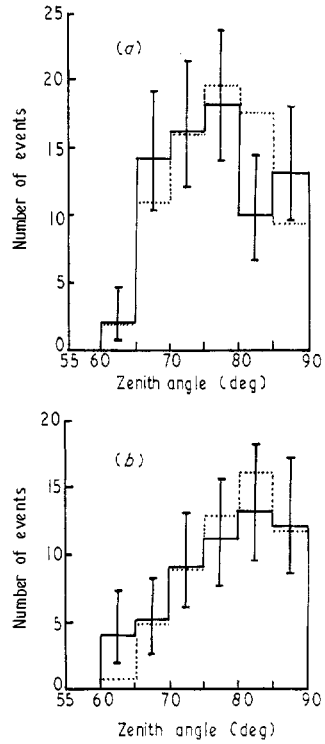

Figure 5. Angular distribution of bursts of size (*a*) 10–20 and (*b*) 100–200 equivalent particles measured in S2. The statistical accuracy of the number of events in each cell is represented by the error flag. The broken line is the predicted distribution.

shown in figures 2 and 3. Figures 4 and 5 show the angular distribution of bursts of size 10 to 20 equivalent particles and 100 to 200 equivalent particles recorded by S1 and S2 respectively.

3. Muon energy spectrum, electromagnetic interaction processes, electron–photon shower curves, and nuclear cascade curves

3.1. *Muon energy spectrum*

In order to calculate the expected burst spectra, the energy spectrum of muons ($E_\mu > 3$ GeV) in the zenith angle range 50–90° must be known. The calculated

spectra of Osborne (1966) are in good agreement with available experimental data, and these spectra have been adopted for $\theta \geqslant 77{\cdot}5^\circ$ and $E_\mu < 1000$ GeV. For θ in the range 50–77·5° the calculated spectra of Allen and Apostolakis (1961) have been used for $E_\mu < 100$ GeV. At higher energies the calculations of Zatsepin and Kuzmin (1961) in conjunction with the Osborne *et al.* (1964) vertical muon spectrum have been used.

3.2. *Electromagnetic interaction processes*

The known electromagnetic processes contributing to the measured bursts are μ–e collisions, direct electron pair production, bremsstrahlung, and nuclear interactions. The probability per g cm^{-2} for a muon of energy E_μ to lose energy in the range vE_μ to $(v+\mathrm{d}v)\,E_\mu$ for the first three of these processes has been given by Rossi (1952):

3.2.1. μ–e *collisions*

$$P(E_\mu, v)\,\mathrm{d}v = \frac{2Cm_e c^2}{E_\mu}\frac{1}{v^2}\left(1 - v + \frac{v^2}{2}\right)\mathrm{d}v.$$

3.2.2. *Direction electron pair production*

$$P(E_\mu, v)\,\mathrm{d}v = \frac{8}{\pi}\alpha^2\frac{N}{A}Z^2 r_e{}^2 H(E_\mu, v, \mu)\,\mathrm{d}v.$$

3.2.3. *Bremsstrahlung*

$$P(E_\mu, v)\,\mathrm{d}v = \alpha\frac{N}{A}Z^2 r_e{}^2\left(\frac{m_e}{m_\mu}\right)^2\frac{16}{3}\left(\frac{3}{4}v + \frac{1-v}{v}\right)F(E_\mu, v)\,\mathrm{d}v$$

where

$$F(E_\mu, v) = \left\{\ln\left(\frac{12}{5}\frac{1-v}{v}\frac{E_\mu}{m_\mu c^2 Z^{1/3}}\right) - \frac{1}{2}\right\}.$$

For fractional energy transfer

$$v \leqslant \frac{1}{r_a}\frac{h}{m_\mu c^2}\frac{E_\mu}{m_\mu c^2}$$

or $v \leqslant 1$ whichever is the smaller

$$F(E_\mu, v) = \left\{\ln\left(\frac{r_a}{r_n}\right) - 1{\cdot}64\right\}$$

where r_a is the Thomas–Fermi radius of the atom and r_n is the nuclear radius. The latter value of $F(E_\mu, v)$ takes into account the effect of electrons in screening the nuclear charge seen by high energy muons at large impact parameters.

3.2.4. *Nuclear interactions.* The expression for nuclear interactions has been taken from Hayman *et al.* (1963)

$$P(E_\mu, v)\,\mathrm{d}v = \frac{2N\alpha\sigma}{\pi}\frac{\ln v\,\mathrm{d}v}{v}$$

where a constant photonuclear cross section $\sigma = 2{\cdot}6 \times 10^{-28}$ cm^2/nucleon is assumed.

3.3. *Electron–photon shower curves*

The information required here is graphs of the total number of electrons and photons and their energy spectra as a function of the distance from the point of

production of high energy electrons and photons in an iron absorber. Graphs of the total number of electrons as a function of depth in electron and photon initiated showers have been calculated by Ivanenko and Samosudov (1959). These calculations seem to be in agreement with experiment for showers with energy of the order of 100 GeV (Murzin and Rappaport 1965, Takbaev *et al.* 1965) and have been adopted in the present work. However Ivanenko and Samosudov (1959) have not calculated the energy spectrum of electrons at a given depth nor do they give the total number of photons and their energy spectrum. These effects have been estimated using approximation A shower theory (Rossi 1952) as a guide and the curves finally adopted for showers initiated by electrons and photons are shown in figures 6 and 7.

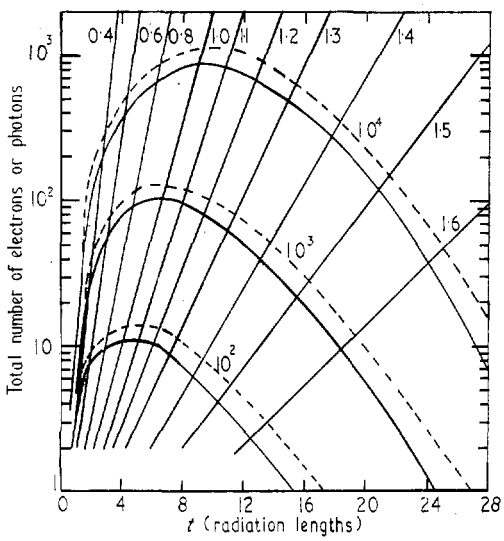

Figure 6. Shower development curves giving the number of electrons (full lines) and photons (broken lines) for cascades in iron initiated by electrons of energies $E/\mathscr{E} = 10^2, 10^3$ and 10^4. The full lines are according to Ivanenko and Samosudov (1959) and the broken lines have been interpolated from approximation A shower theory. The straight lines are the loci of constant age parameter s.

The pulse height recorded by the scintillators in the present experiment is a measure of the total track length of ionizing particles in the phosphors. Some electrons traverse the phosphor completely, some stop, and photons produce electrons by the Compton and pair production processes. To account for this the energy spectrum of electrons and photons has been taken to be of the form

$$N(>E) = N(1+E/\mathscr{E})^{-s}$$

where N is the total number of photons or electrons and $\mathscr{E}$ is the critical energy. With this information and the data of figures 6 and 7 the burst size in equivalent particles has been calculated for primary electron and photon showers as a function of the distance of the point of production of the electron or photon from the phosphor. The result is shown in figure 8 for showers whose axes are incident normally on the phosphor. The effect of photon interactions in the phosphor is to increase the calculated burst size by 24%. One equivalent particle is defined as the average pulse height produced by a relativistic muon traversing the phosphor at

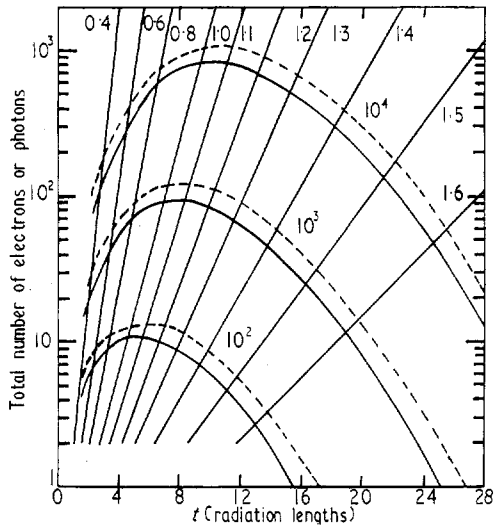

Figure 7. Shower development curves giving the number of electrons (full lines) and photons (broken lines) for cascades initiated in iron by photons of energies $E/\mathscr{E} = 10^2$, 10^3 and 10^4. The full lines are according to Ivanenko and Samosudov (1959) and the broken lines have been interpolated from approximation A shower theory. The straight lines are the loci of constant age parameter s.

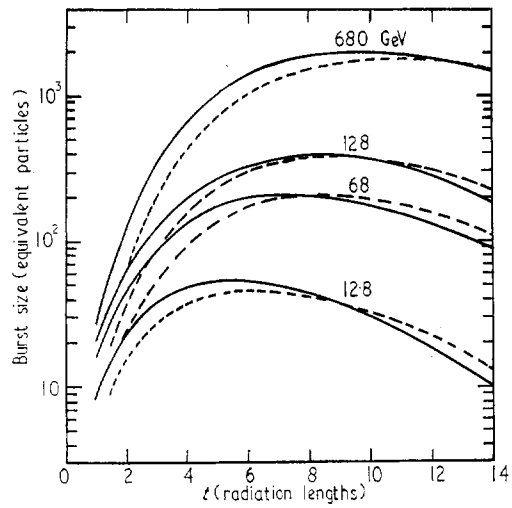

Figure 8. Shower development curves for cascades initiated by primary electrons (full lines) and primary photons (broken lines). The burst size is in terms of the equivalent number of particles recorded by the scintillators S1 and S2 for showers whose axes are incident on them normally.

normal incidence. For showers incident at non-normal incidence other cascade curves were calculated similar to that shown in figure 8. In using the cascade curves the radiation length t in iron, and critical energy $\mathscr{E}$ have been taken to be 14·1 g cm^{-2} and 21 MeV respectively.

3.4. *Nuclear cascade curves*

A muon undergoing a nuclear interaction in the iron targets will produce charged and neutral pions. The charged pions will decay within negligible distance into two γ rays and initiate an electron–photon cascade. Some of the charged pions produced will interact before leaving the target and again the neutral pions will initiate an electron–photon cascade. Again, curves of the total track length of ionizing particles in the scintillator phosphor as a function of the distance of the point of the nuclear interaction from the phosphor are required for a range of interaction energies. To calculate these curves it has been assumed that the total multiplicity n of pions produced by the interaction of a virtual photon of energy E GeV is $n = 3E^{1/4}$ and that $\frac{1}{3}$ of the produced pions are neutral. Equipartition of energy among the produced pions is assumed and an interaction length of charged pions in iron of 19·3 cm has been used and again a total multiplicity of $3E^{1/4}$ assumed. The result of the calculation for cascades incident normally on the phosphor is shown in figure 9.

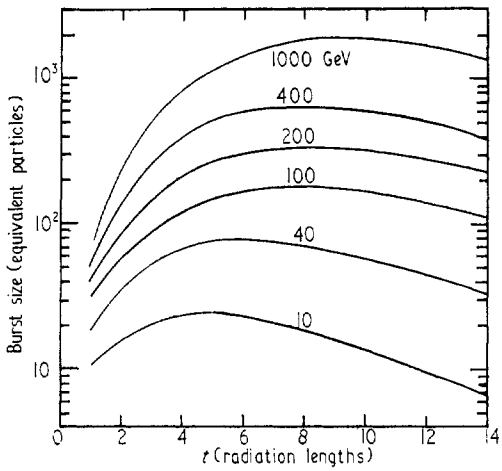

Figure 9. Cascade curves for the nuclear interactions of muons producing the indicated energy transfers. The curves are for showers whose axes are incident normally on the scintillators S1 and S2.

4. The expected burst spectra

If $N(E_\mu, \theta)\,\mathrm{d}E_\mu$ is the differential energy spectrum of muons at zenith angle θ through the apparatus then the differential energy transfer production spectrum per g cm^{-2} of iron due to any one of the electromagnetic processes is given by

$$N(E_t, \theta)\,\mathrm{d}E_t = \int_{E_{\mu\,\min}}^{\infty} N(E_\mu, \theta) F(E_\mu, E_t)\,\mathrm{d}E_t\,\mathrm{d}E_\mu$$

where $E_{\mu\,\min}$ is the minimum muon energy capable of producing an energy transfer E_t. $F(E_\mu, E_t)\,\mathrm{d}E_t$ is the probability that a muon of energy E_μ produces an energy transfer in the range E_t to $E_t + \mathrm{d}E_t$. The first step in the calculations was thus to calculate the differential energy transfer production spectrum per g cm^{-2} of iron due to knock-on electrons, direct pair production, bremsstrahlung and nuclear interactions for a variety of zenith angles. For each zenith angle the burst spectrum due to each

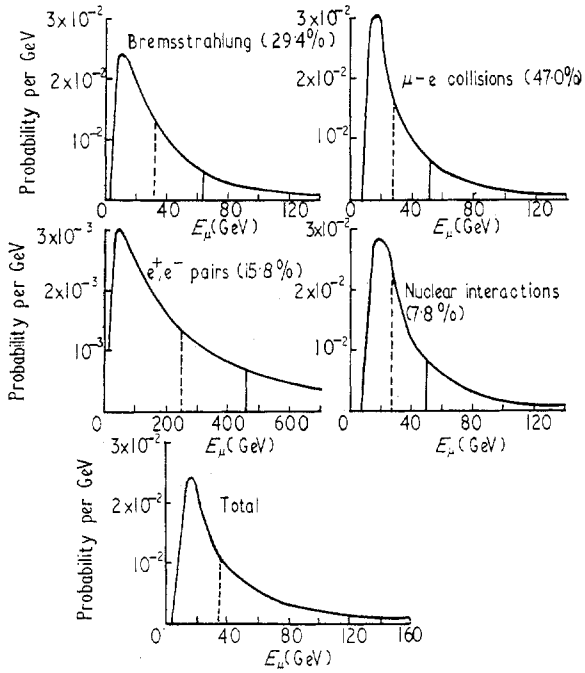

Figure 10. Distribution of muon energies producing a burst of 13·2–26·4 equivalent particles in S1 for the different interaction processes. The figures in parenthesis are the relative contributions of each process to the total. The broken and full line ordinates represent the median and mean muon energies respectively.

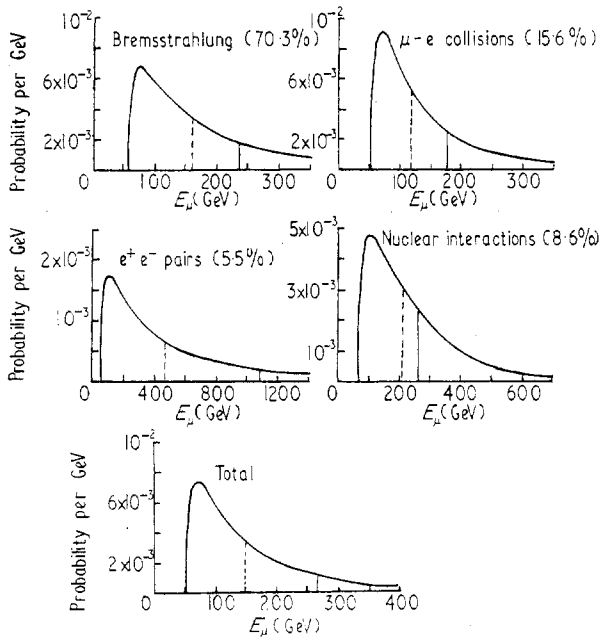

Figure 11. Distribution of muon energies producing a burst of 132–264 equivalent particles in S1 for the different interaction processes. The figures in parenthesis are the relative contributions of each process to the total. The broken and full line ordinates represent the median and mean muon energies respectively.

process could then easily be calculated using the shower development curves shown in figures 8 and 9. As a final step the contribution of each process to the measured burst spectrum was found by integrating over the range of accepted zenith angles. The results are shown in figures 2 and 3. From these calculations the expected angular distribution of bursts in the range 10–20 and 100–200 equivalent particles was also found and the measurements are compared with expectation in figures 4 and 5.

Various items of interest can be extracted from the calculations described. Figures 10 and 11 show the energy distribution of muons producing burst sizes in the range 13·2–26·4 and 132–264 equivalent particles respectively. Figure 12 shows the

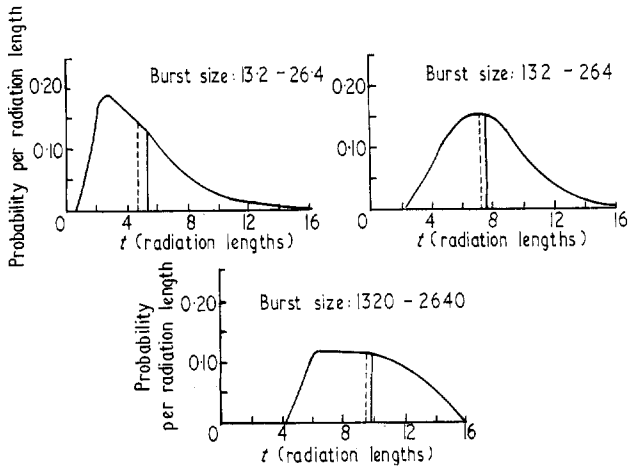

Figure 12. Depth probability distributions for various burst sizes in S1. Each abscissa is the distance from S1 in radiation lengths at which an interaction occurs, the resulting shower producing a burst in S1 in the size range indicated. The broken and full line ordinates represent the median and mean muon energies respectively.

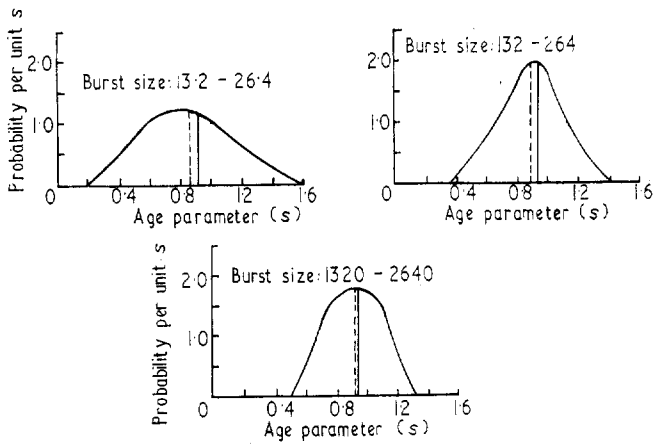

Figure 13. Distribution of age parameter (s) for various burst sizes in S1. The broken and full line ordinates represent the median and mean muon energies respectively.

probability distribution of the distance of the point of interaction in the target from the phosphor for various burst size ranges and figure 13 shows the distribution of age parameter s for various burst sizes in S1. Finally, figure 14 shows the median energy transfer and median muon energy producing a given burst size in S1 and S2.

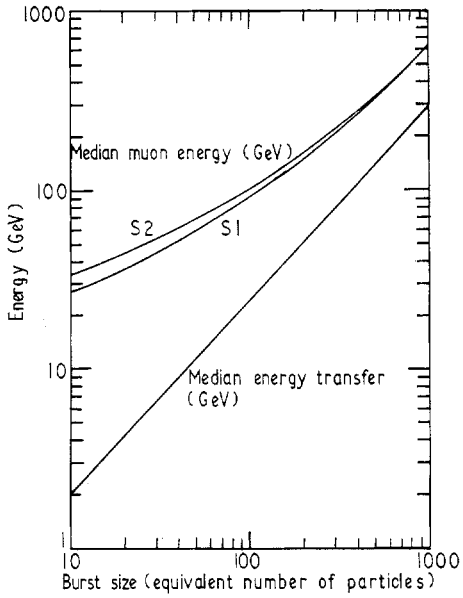

Figure 14. Relation between burst size, median energy transfer and median muon energy for bursts measured in S1 and S2.

5. Fluctuations

Takbaev *et al.* (1965) have examined the distribution of charged particles in cascades with energy of the order of 100 GeV produced in iron by means of an ionization calorimeter and reached the following conclusions:

(i) At small thicknesses ($t < 2$ radiation lengths) the distribution approximates to Furry.

(ii) Near shower maximum the distribution is normal.

(iii) At large thicknesses ($t > 17$ radiation lengths) the distribution approximates to Poisson.

The data of Crawford and Messel (1965) also shows the same form as observed by Takbaev *et al.* (1965), being a minimum at shower maximum and becoming larger for small and large depths in the shower. Both these results are in agreement with the calculations of Gerasimova (1964). Near the beginning of the shower, there are a few highly energetic particles, so that fluctuations are significant for the development of the shower. These fluctuations, particularly for photon induced showers are close to Furry. Near shower maximum, the fluctuations are smaller due to the larger number of particles present.

From figures 12 and 13 it is seen that even bursts of small size are produced predominantly by showers close to the maximum of their development. Thus it is reasonable to expect that Poisson fluctuations (which become Gaussian for large numbers of particles) would give a reliable estimate of the effect of fluctuations on

the predicted burst spectrum. Carrying out the necessary calculations on the total predicted burst spectrum shown in figures 2 and 3 shows that neither the absolute predicted intensity nor the shape of the distribution is altered by the occurrence of such fluctuations.

6. Conclusions

It can be seen from figures 2, 3, 4 and 5 that there is no significant discrepancy between theory and experiment for the measurements of the shape and absolute magnitude of the differential burst spectra as well as for the angular distribution of bursts of a given size. The precision of the measurements is $\pm 10\%$ for energy transfers of 3·6 GeV (produced predominantly by μ–e collisions) generated by muons of median energy 34 GeV, and $\pm 30\%$ for energy transfers of 240 GeV (produced predominantly by bremsstrahlung) generated by muons of median energy 520 GeV).

Acknowledgments

Professor G. D. Rochester and Professor A. W. Wolfendale are thanked for encouraging this work. The work was supported by a grant from Research Corporation which is gratefully acknowledged.

References

ALLEN, J. E., and APOSTOLAKIS, A. J., 1961, *Proc. R. Soc.* A, **265,** 117–32.

ASHTON, F., and COATS, R. B., 1965, *Proc. Int. Conf. on Cosmic Rays,* Vol. 2 (London: The Institute of Physics and The Physical Society), pp. 959–61.

ASHTON, F., COATS, R. B., and SIMPSON, D. A., 1965, *Proc. Int. Conf. on Cosmic Rays,* Vol. 2 (London: The Institute of Physics and The Physical Society), pp. 1079–81.

—— 1968, *Can. J. Phys.*, **46,** S361–4.

ASHTON, F., *et al.*, 1966, *Proc. Phys. Soc.*, **87,** 79–88.

ASHTON, F., and WOLFENDALE, A. W., 1963, *Proc. Phys. Soc.*, **81,** 593–603.

CRAWFORD, D. F., and MESSEL, H., 1965, *Nucl. Phys.*, **61,** 145–76.

GERASIMOVA, N. M., 1964, *Bull. Acad. Sci., USSR.*, **28,** 1758–60.

IVANENKO, I. P., and SAMOSUDOV, B. E., 1959, *Sov. Phys.-JETP*, **8,** 884–7.

JAKEMAN, D., 1956, *Can. J. Phys.*, **34,** 432–50.

MURZIN, V. S., and RAPPAPORT, I. D., 1965, *Sov. Phys.-JETP*, **20,** 1–3.

OSBORNE, J. L., 1966, *Ph D Thesis*, Durham University.

OSBORNE, J. L., WOLFENDALE, A. W., and PALMER, N. S., 1964, *Proc. Phys. Soc.*, **84,** 911–3.

ROSSI, B., 1952, *High Energy Particles* (New York: Prentice-Hall).

TAKBAEV, ZH. S., LUKIN, YU. T., and EMELYANOV, Yu. A., 1965, *Proc. Int. Conf. on Cosmic Rays* Vol. 2 (London: The Institute of Physics and The Physical Society), pp. 967–8.

ZATSEPIN, G. T., and KUZMIN, V. A., 1961, *Sov. Phys.-JETP*, **12,** 1171–7.